PHYSICAL REVIEW C VOLUME 13, NUMBER 4 APRIL 1976

Spectroscopic and reaction mechanism information derived from ^{160}Gd(d, t)^{159}Gd and ^{162}Dy(d, t)^{161}Dy reaction measurements*

J. C. Peng, J. V. Maher, G. H. Wedberg, and C. M. Cheng
University of Pittsburgh, Pittsburgh, Pennsylvania 15260
(Received 11 December 1975)

Angular distributions have been measured for transitions populating residual states of ^{159}Gd and ^{161}Dy through the (d, t) reaction at $E_d = 17$ MeV. Many of these angular distributions have shapes which are well reproduced by distorted-wave Born-approximation calculations which assume orbital angular momentum transfers l which are compatible with the previously assigned spin-parities of the states. But a significant number of angular distributions are anomalous; i.e., either they cannot be fitted by any reasonable distorted-wave Born-approximation calculation or they can only be fitted with a calculation which assumes an l value incompatible with the previous Nilsson model assignment of the state. While the summed spectroscopic factors are in good agreement with Nilsson model expectations, the spectroscopic factors for many levels deviate significantly from Nilsson model predictions—even though Coriolis coupling has been included in the model calculation. The observation of several strongly anomalous angular distributions along with some anomalous oscillatory large-angle structure in many additional angular distributions and large discrepancies between observed and model-predicted spectroscopic factors almost certainly indicates that the assumption of a simple one-step direct reaction mechanism breaks down for these reactions.

[NUCLEAR REACTIONS ^{160}Gd(a,t), ^{162}Dy(d,t), E_d=17 MeV, measured $\sigma(\theta)$; DWBA analysis, deduced levels, l values, spectroscopic factors. Enriched targets.]

I. INTRODUCTION

The limits of applicability of direct reaction assumptions are not well established and the investigation of these limits has motivated many recent investigations.[1-3] Unfortunately, since distorted-wave Born-approximation (DWBA) calculations are easily performed and the next most reasonable improvement—the coupled-channels Born-approximation (CCBA) calculation—is much more difficult to perform, there has been a tendency to vary parameters to fit as much data as possible with DWBA and to apply CCBA only in an *ad hoc* fashion to troublesome cases of experimental data. This difficulty in defining the limits of applicability of the DWBA is exacerbated by problems of acquiring a data base. Multinucleon transfer reactions frequently stretch the DWBA assumptions, but for such reactions it is not possible to separate structure from kinematic factors in the DWBA calculations so the analysis procedure is less reliable than for single-nucleon transfer reactions where structure and kinematic factors are algebraically separable. On the other hand, multistep effects in single-nucleon transfer reactions appear to be small for most cases of spherical nuclides.[4] The study of (d,t) reactions on deformed rare-earth targets provides an excellent opportunity to acquire an extensive set of data for which the DWBA assumptions should be marginal and for which the DWBA analysis should be reasonably straightforward. Both the deuteron and the triton are strongly absorbed and at least for most transitions in spherical nuclides, (d,t) angular distributions are smooth diffraction patterns which are easily fit with DWBA calculations that use reasonable optical model parameter sets. The splitting of single-particle states in deformed nuclei provides, in any one deformed residual nucleus, a multiplicity of states of each spin, in most of which the amplitudes for population by direct single-particle transfer are sufficiently small that multistep effects might be detectable.[5,6]

This work is part of a larger investigation into the mechanism of the (d,t) reaction on six neighboring deformed even-even targets (^{160}Gd, ^{162,164}Dy, ^{166,168}Er, and ^{170}Yb). In a previous paper,[7] we have reported evidence for systematic violations of one-step direct reaction assumptions in certain single-particle states in all targets studied—i.e., DWBA analysis of the observable transitions to members of the $\frac{11}{2}^-[505]$, $\frac{3}{2}^-[521]$, $\frac{1}{2}^-[521]$, and $\frac{5}{2}^+[642]$ Nilsson bands shows anomalous spectroscopic factors and/or anomalous angular distribution shapes for transitions to some members of each of these bands in nearly all residual nuclides which were studied. The transitions discussed in Ref. 7 were restricted to low-lying states of reasonably well established spin-parity where there is no doubt of expected orbital angular momentum transfer (l) and where unaccounted vibrational couplings should have minimum

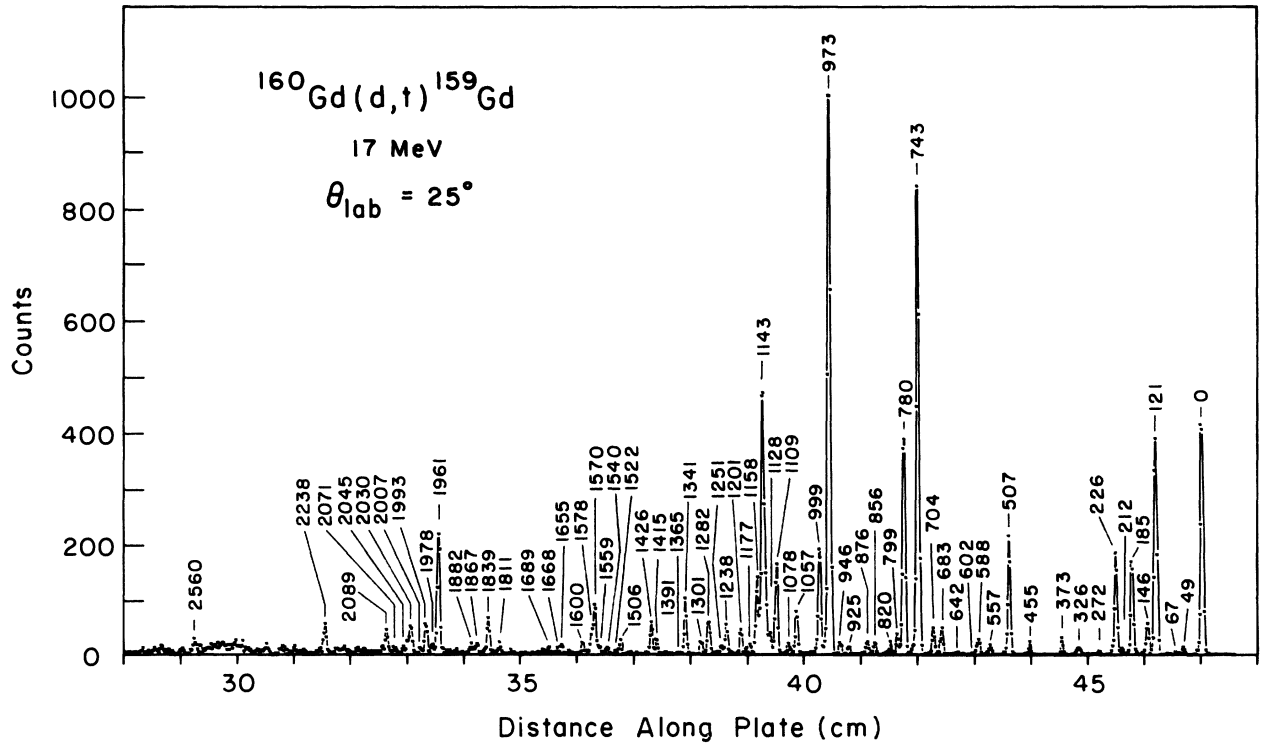

FIG. 1. Spectrum of tritons from the ^{160}Gd$(d,t)^{159}$Gd reaction measured at $\theta_{lab}=25°$. Excitation energies of residual ^{159}Gd states are listed in keV.

effects on Nilsson model predictions of single-particle strengths. This paper presents both reaction mechanism and spectroscopic results for all the observed transitions in our study of the (d,t) reaction on the $N=96$ isotones ^{160}Gd and ^{162}Dy. Some spectroscopic information was previously available for both residual nuclei: both ^{159}Gd and ^{161}Dy have been studied through (d,p) and (d,t) reactions induced with 12 MeV deuterons.[8-10] Most transitions were only observed in two or three spectra,[8,9] but angular distributions were measured[10] for some of the transitions to levels in ^{159}Gd. A ^{162}Dy(^{3}He, α)^{161}Dy spectrum has also been reported.[11] The spins and parities (J^π) of the low excitation energy states of both nuclides have been reasonably well established through γ decay studies,[12-15] but the J^π values for most levels have been assigned by comparing (d,p) and (d,t) spectra with "signatures" deduced from DWBA calculations using spectroscopic factors predicted by the Nilsson model (without inclusion of Coriolis coupling).[8,9]

The data of the present investigation have been analyzed with finite range nonlocal DWBA calculations. The intent of this analysis is to organize the data for comparison with Nilsson model expectations as to orbital angular momentum transfer (l) and spectroscopic strength. Since, between the Nilsson model and the DWBA calculations, there are many possible parameters which could be varied, an attempt has been made to standardize the analysis parameters with the best available information rather than make *ad hoc* parameter variations to fit data for individual transitions. The selection of parameters is discussed for the DWBA calculations in Sec. III and for the calculations of Nilsson model spectroscopic factors in Sec. IV. It has not been possible to perform CCBA calculations, but it is hoped that the present results will provide a reasonably extensive data base for CCBA calculations to investigate under what spectroscopic/reaction dynamic conditions the assumption of a one-step direct transfer mechanism breaks down.

II. DATA ACQUISITION AND REDUCTION

The experiment was performed with 17 MeV deuterons from the Pittsburgh three stage van de Graaff accelerator. The targets were ~75 μg/cm^2 metallic foils evaporated on carbon and aluminum backings. The Gd foils were enriched to >99.9% ^{160}Gd and the Dy to 96.3% ^{162}Dy. Tritons from the (d,t) reaction were detected in emulsions placed in the focal plane of a split-pole spectrograph (whose acceptance solid angle was

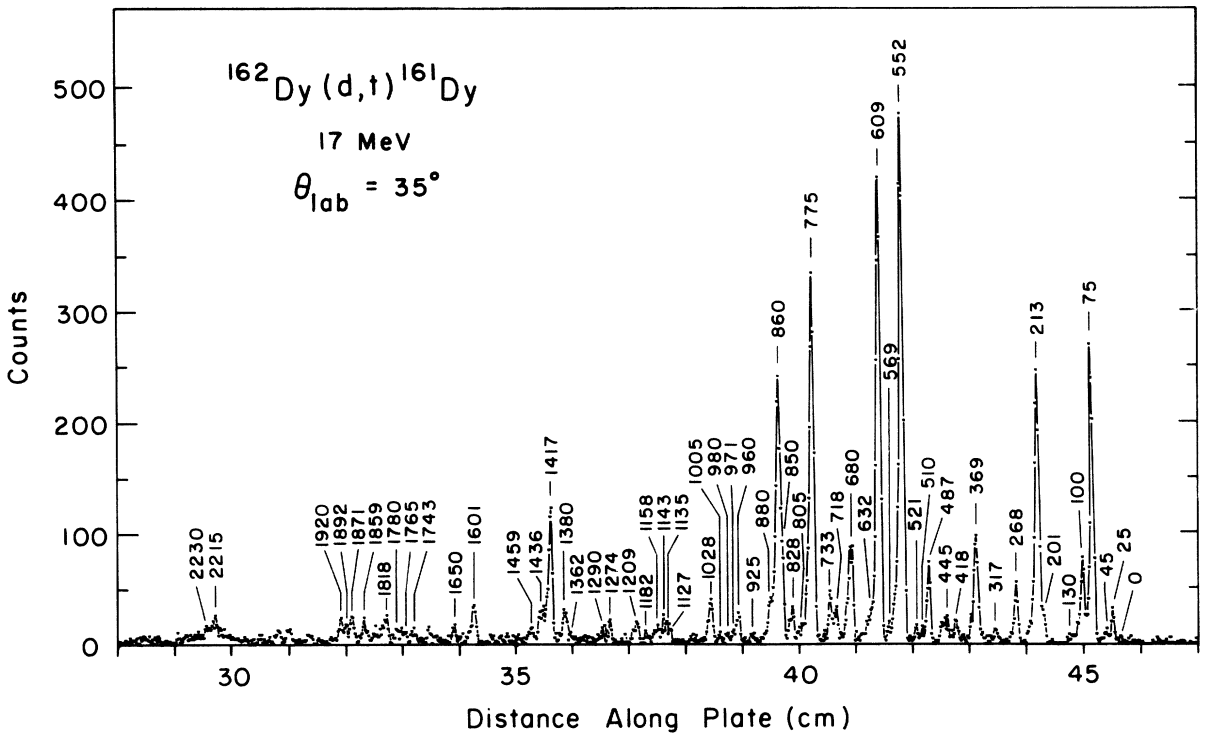

FIG. 2. Spectrum of tritons from the ^{162}Dy$(d,t)^{161}$Dy reaction measured at $\theta_{lab}=35°$. Excitation energies of residual ^{161}Dy states are listed in keV.

set at 1.4 msr). The developed plates were scanned by the Argonne automatic plate scanner[16]; some were checked by human scanners. Typical spectra are shown in Figs. 1 and 2. The energy resolution was ~7 keV for the ^{160}Gd spectra and ~10 keV for the ^{162}Dy spectra. Two NaI detectors were set at $\theta_{lab}=\pm 38°$ to monitor possible target deterioration. ^{160}Gd$(d,t)^{159}$Gd transitions were measured at 14 angles over the range $10° \leq \theta_{lab} \leq 60°$. At several angles two measurements dif-

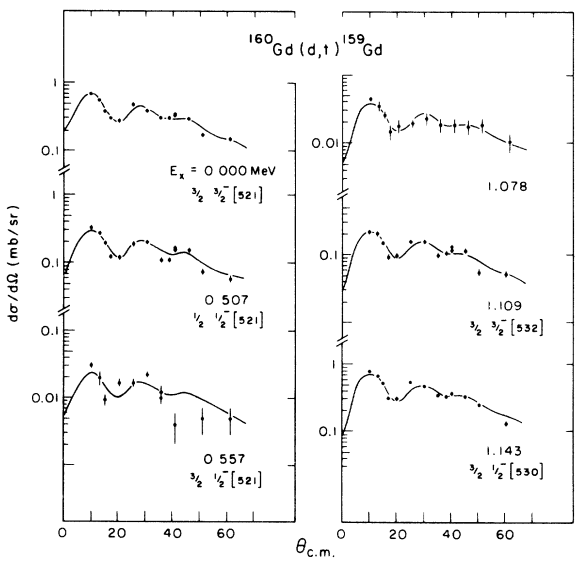

FIG. 3. $l=1$ angular distributions from the ^{160}Gd(d,t)-^{159}Gd reaction. The solid curves are DWBA calculations.

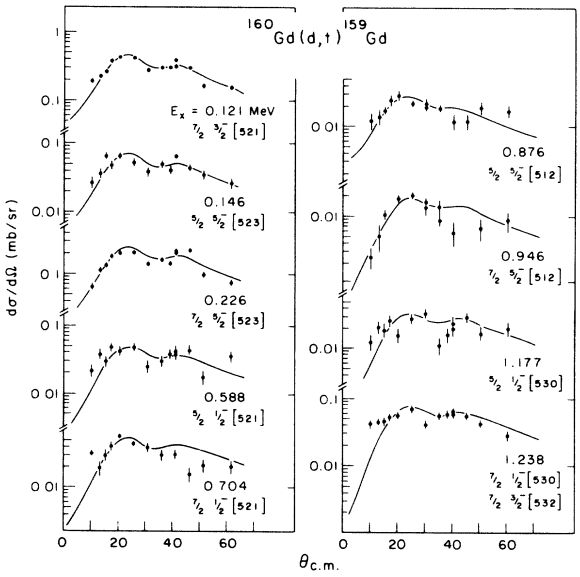

FIG. 4. $l=3$ angular distributions from the ^{160}Gd(d,t)-^{159}Gd reaction. The solid curves are DWBA calculations.

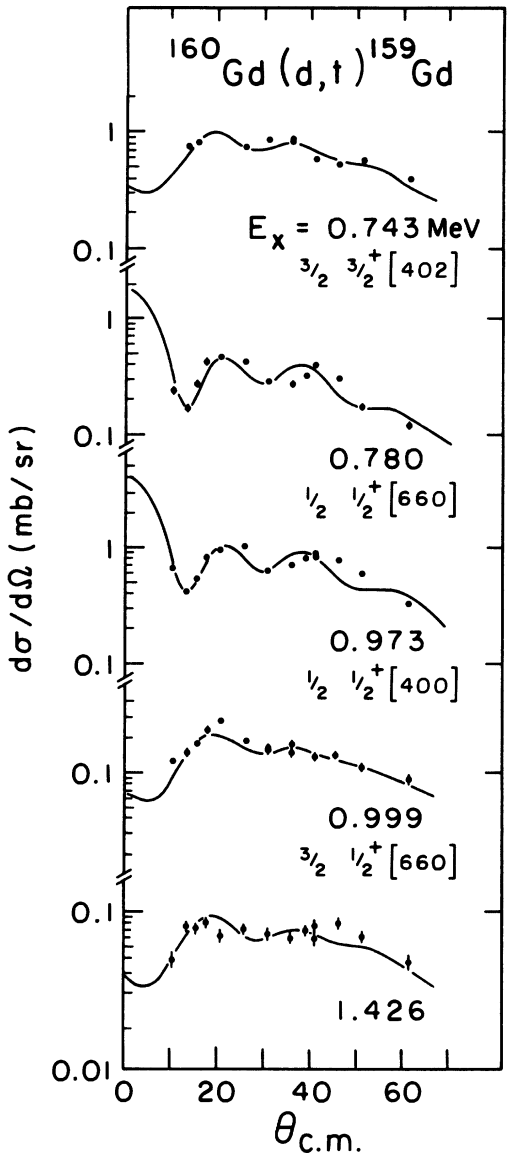

FIG. 5. $l=0$ and $l=2$ angular distributions from the ^{160}Gd$(d,t)^{159}$Gd reaction. The solid curves are DWBA calculations.

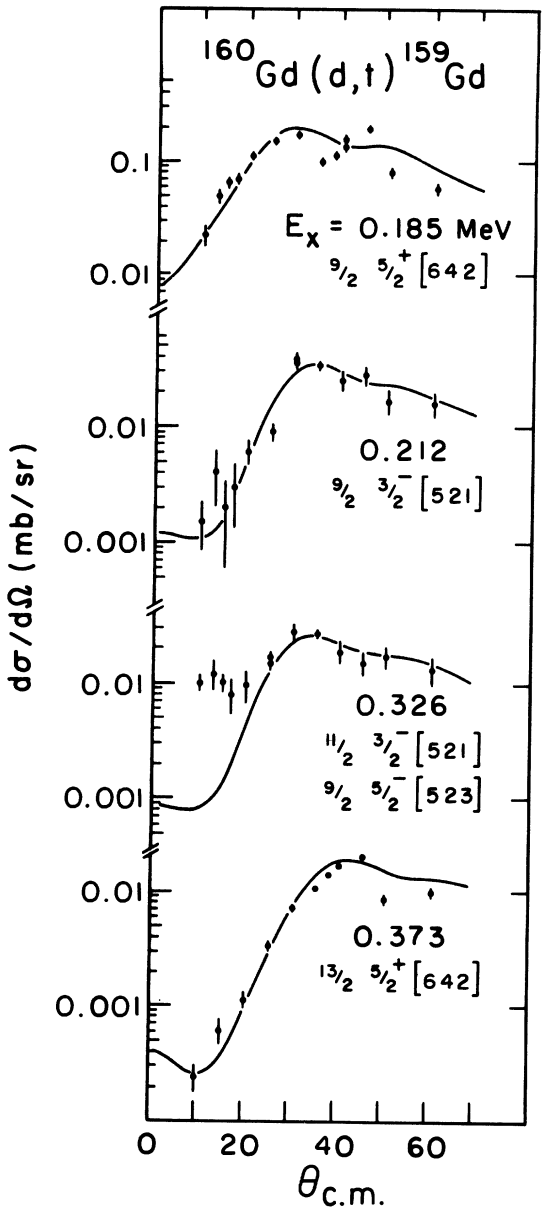

FIG. 6. $l \geq 4$ angular distributions from the ^{160}Gd$(d,t)^{159}$Gd reaction. The solid curves are DWBA calculations.

fering in beam charge integration ($q=1$ and 3 mC, respectively) were necessary since several strong transitions overexposed the emulsions during the long exposure required to measure the majority of the interesting transitions. ^{162}Dy$(d,t)^{161}$Dy transitions were measured at 15 angles in the range $8° \leq \theta_{lab} \leq 50°$.

Peak areas were extracted from the spectra with the peak-fitting code AUTOFIT.[17] The reliability of the fitting procedure was ensured by numerous hand checks. The resulting angular distributions are shown for ^{160}Gd$(d,t)^{159}$Gd transitions in Figs. 3–8 and for ^{162}Dy$(d,t)^{161}$Dy transitions in Figs. 9–15.

Elastic scattering cross sections for 17 MeV deuterons on ^{162}Dy, ^{164}Dy, ^{166}Er, and ^{168}Er were measured with a surface barrier detector in 2° steps over an angle range $10° \leq \theta_{lab} \leq 90°$. These elastic scattering angular distributions are shown in Fig. 16.

Not only were these data fitted with an optical potential (using the code GENOA[18]) which is presented below, but they also determined the abso-

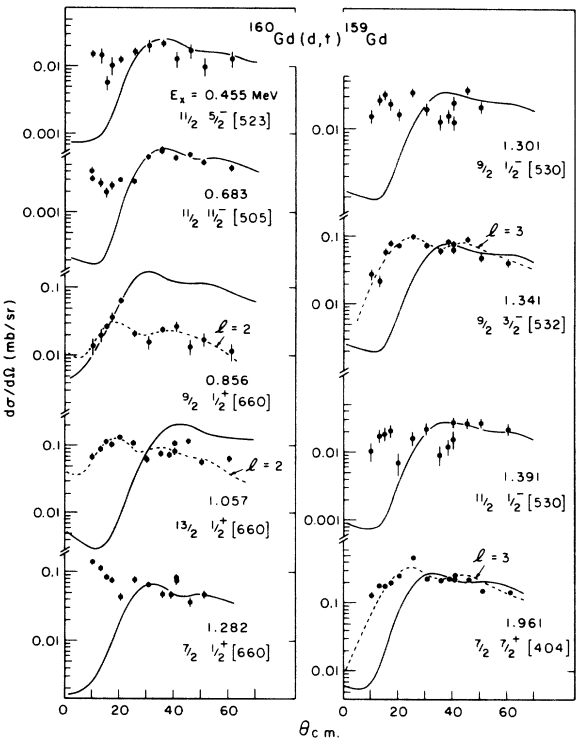

FIG. 7. Anomalous angular distributions from the ^{160}Gd$(d,t)^{159}$Gd reaction. The solid curves are DWBA calculations for an l value compatible with the indicated Nilsson model assignment. The dashed curves (discussed in text) are DWBA calculations which assume an l value which is incompatible with the Nilsson model assignment of the state.

lute elastic scattering cross sections at the position of the NaI monitor detectors which in turn could be used to determine the absolute cross sections of the (d,t) transitions. These latter absolute cross sections should be accurate to ±15%.

III. DWBA CALCULATIONS AND ANGULAR DISTRIBUTION SHAPES

The code DWUCK[19] was used to perform the finite range nonlocal DWBA calculations described in this section. Table I lists the optical potential parameters and bound state potential parameters used in these calculations. The finite range parameter was set at 0.845 and nonlocality parameters at 0.54 (for the deuteron) and 0.25 (for the triton). The triton optical parameters are those of Flynn *et al.*[20] Two sets of deuteron optical potential parameters are listed in Table I. The first set resulted from a global fit to deuteron scattering (mostly on spherical nuclei) by Perey and Perey.[21] In order to test the sensitivity of the DWBA calculations to changes in optical potential parameters a second potential was deter-

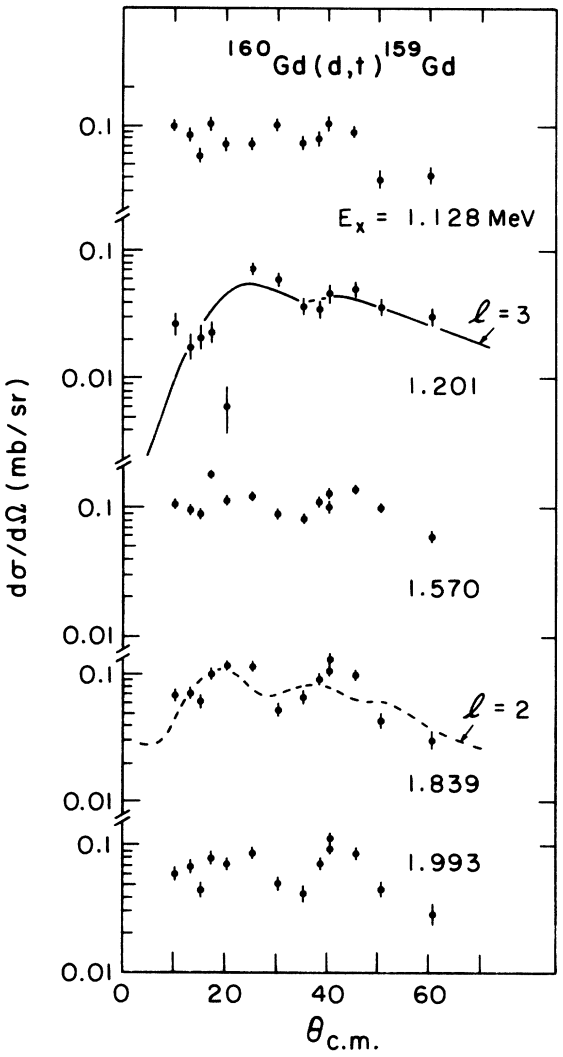

FIG. 8. Angular distributions for strong ^{160}Gd(d,t)-^{159}Gd transitions to states of unknown spin at large excitation energy.

mined by fitting the elastic scattering data shown in Fig. 16 with the optical model search code GENOA.[18] The geometry of the real potential was fixed in this fitting procedure and the starting value of the real well depth was chosen near 100 MeV so the resulting potential matches[22] properly with the triton and bound state neutron potentials. No significant differences were found between DWBA calculations performed with the two deuteron potentials. All spectroscopic information presented below was extracted with DWBA calculations which used the Perey potential.[21]

Some of the transitions of interest in this experiment involve total angular momentum transfer values which, when used with the binding energy prescription in DWBA calculations, result in un-

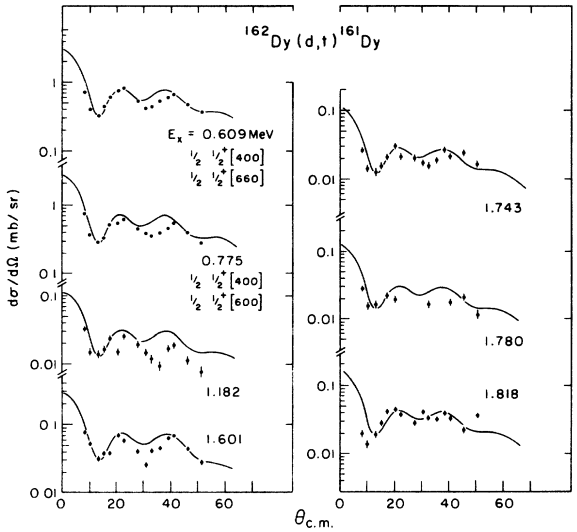

FIG. 9. $l=0$ angular distributions from the ^{162}Dy(d,t)-^{161}Dy reaction. The solid curves are DWBA calculations.

reasonably shallow or deep bound state well depths (depending on which radial quantum number n is selected). This is a well-known problem which occurs in spherical nuclei for states of weak single-particle (or hole) character far separated from the centroid of their subshell.[23] The problem is more severe in deformed nuclei because the single-particle fragmentations that result from breaking spherical symmetry can place significant single-particle strength in an orbital whose binding energy is very different from that of the nearest spherical model orbital of the same spin and parity. Since DWBA expectations are known to have weak dependence on total angular momentum transfer (j), the experimental angular distributions have been fitted with the proper orbital angular momentum transfer (l) but with the n and j values which keep the potential well depth in the bound state calculation near 60 MeV. Table II lists the nlj values employed in this analysis. With this procedure bound state well depths were always reasonable.

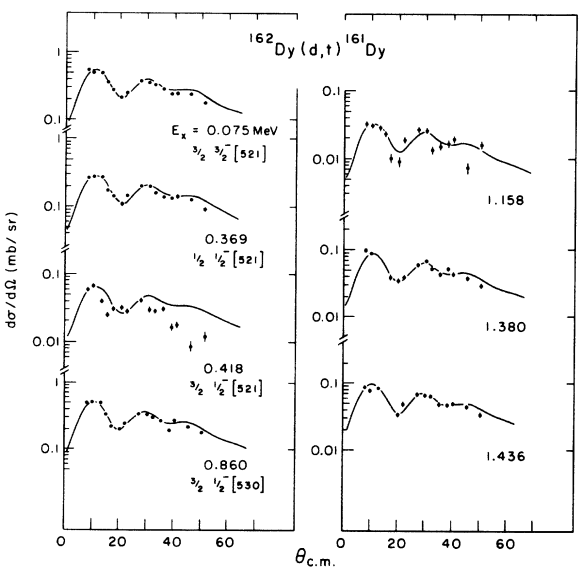

FIG. 10. $l=1$ angular distributions from the ^{162}Dy(d,t)-^{161}Dy reaction. The solid curves are DWBA calculations.

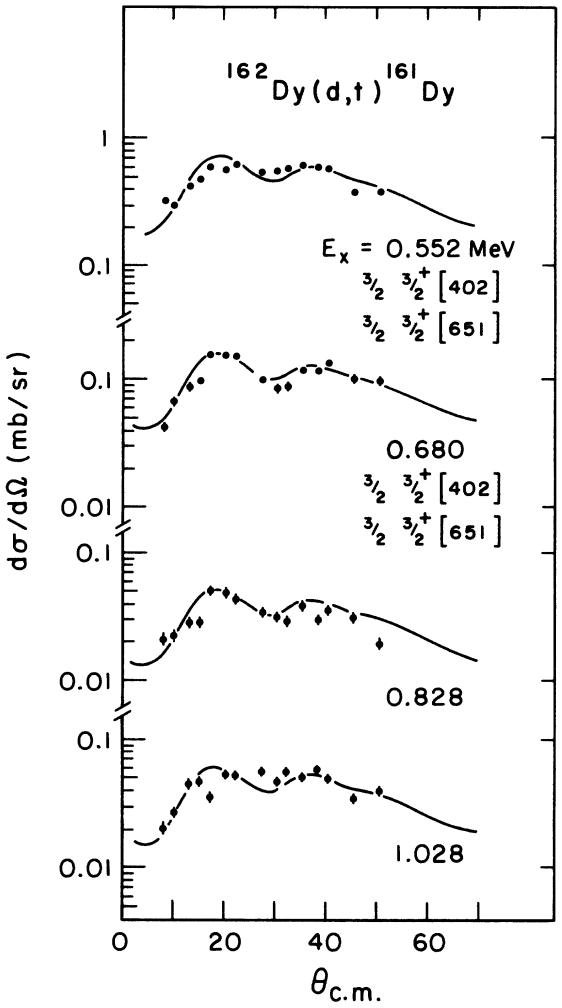

FIG. 11. $l=2$ angular distributions from the ^{162}Dy(d,t)-^{161}Dy reaction. The solid curves are DWBA calculations.

Angular distributions for most of the strong transitions observed in this experiment are well fitted by the DWBA calculations—as can be seen from Figs. 3–6 and 9–12. The $l=0$ DWBA angular distributions (Figs. 6 and 9) show a tendency to be

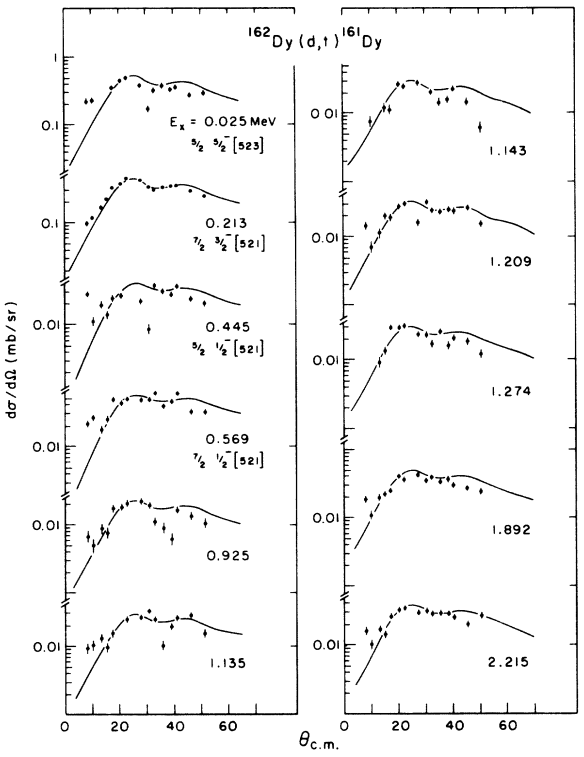

FIG. 12. $l=3$ angular distributions from the ^{162}Dy(d,t)-^{161}Dy reaction. The solid curves are DWBA calculations.

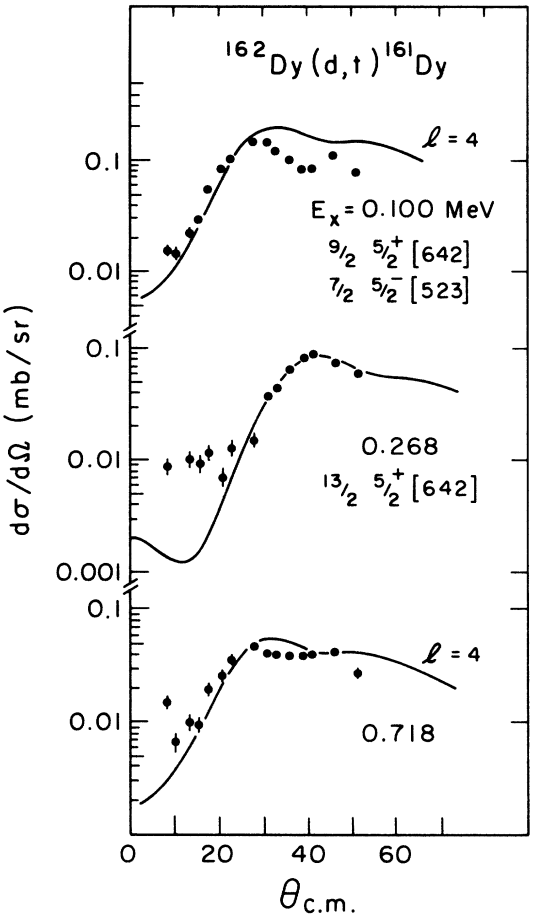

FIG. 13. $l>3$ angular distributions from the ^{162}Dy(d,t)-^{161}Dy reaction. The solid curves are DWBA calculations.

out of phase and less strongly oscillatory than the data at large (>30°) angles. All strong $l=1$ angular distributions are very well fitted (Figs. 3 and 10). $l=2$ and $l=3$ angular distributions (Figs. 4, 5, 11, and 12) are also well fitted, but with a tendency to have small-angle cross sections larger than DWBA predictions. Higher l (≥ 4) transitions (Figs. 6, 7, 13, and 14) pose a problem. These transitions are frequently very well fitted by DWBA calculations, but equally often the data deviate significantly from the DWBA prediction. This can be partially explained in a number of ways: (1) High l transitions are of intrinsically smaller cross section than are low l transitions so any contamination of the process with multistep effects might be expected to produce more dramatic results. (2) The first maximum in high l transfer DWBA angular distributions falls at a large angle. Since angular distributions are normally expected to drop steeply at angles smaller than this maximum, it is easier to identify deviations in high l transfer cases than for low l transfers where the small angle data points fall on or near the first DWBA maximum.

Figures 7, 13, and 14 contain anomalous angular distributions. Some of these can be fitted by DWBA calculations for an l different from that required by the previously reported Nilsson model assignment of the level. This suggests that some of the anomalies can be attributed to misassignments in previous work, but in many cases DWBA calculations cannot fit the angular distribution for any l value.

IV. SPECTROSCOPIC FACTORS AND NILSSON MODEL PARAMETERS

Spectroscopic factors have been extracted from the measured angular distributions by using the relation:

$$\left(\frac{d\sigma}{d\Omega}\right)_{\text{exp}} = 3.33 C^2S \frac{(d\sigma/d\Omega)_{\text{DWBA}}}{(2j+1)},$$

where C^2S is the spectroscopic factor, $(d\sigma/d\Omega)_{\text{exp}}$ is the data, $(d\sigma/d\Omega)_{\text{DWBA}}$ is the DWBA calculation made with the code DWUCK, and j is the angular

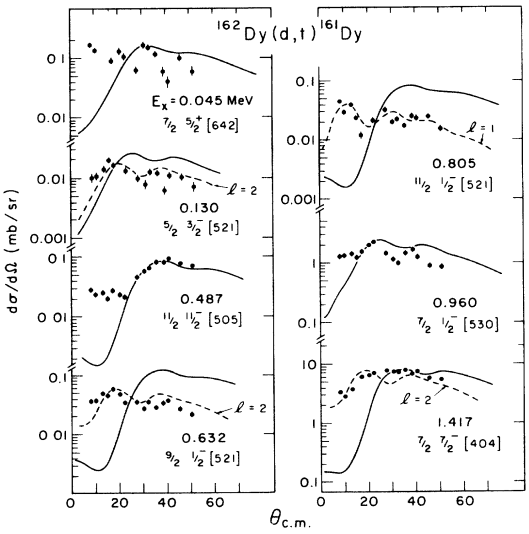

FIG. 14. Anomalous angular distributions from the ^{162}Dy$(d,t)^{161}$Dy reaction. The solid curves are DWBA calculations for an l value compatible with the indicated Nilsson model assignment. The dashed curves (discussed in text) are DWBA calculations which assume an l value which is incompatible with the Nilsson model assignment of the state.

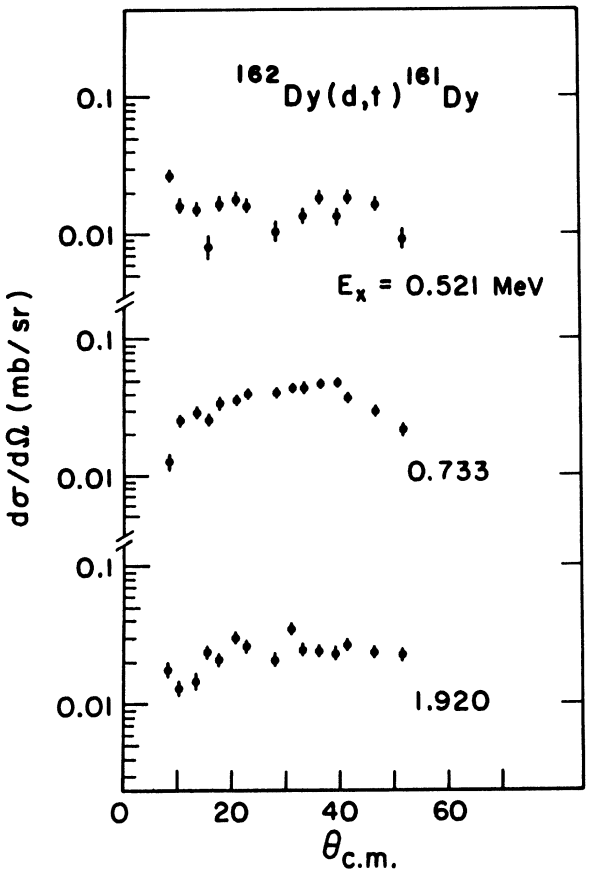

FIG. 15. Angular distributions for strong ^{162}Dy(d,t)-^{161}Dy transitions to states of unknown spin at large excitation energy.

momentum transfer assumed in the calculation. Tables III and IV list, for each level populated in ^{159}Gd and ^{161}Dy, excitation energy, the empirically determined l value, the Nilsson model assignment (where known from previous work), cross section at one angle, and spectroscopic factor. For those levels whose angular distributions show significant deviations from DWBA predictions, the spectroscopic factors are uncertain, representing a normalization of the DWBA prediction to the measured cross section in the angular region of the principal maximum in the DWBA angular distribution. Even for transitions like the $l=5$ transition to the 0.487 MeV state of ^{161}Dy ($\frac{11}{2}\frac{11}{2}^-[505]$) where the DWBA calculation gives a good fit to the data in the region of the principal maximum, the meaning of the extracted spectroscopic factor may be questioned. As discussed below and in the introduction, the DWBA is used in these cases to help organize the data with no strong claim of validity for resulting spectroscopic implications.

Also shown in Tables III and IV are spectroscopic factors predicted by Nilsson model calculations[24] performed with the code BANDFIT.[25] Given an energy spectrum with spin, parity, and Nilsson model quantum numbers assigned to each level, this code will vary any or all of several parameters to fit the energy spectrum and then use the resulting parameters to predict spectroscopic factors for single-nucleon transfer reactions. As BANDFIT was used in this investigation, the parameters of the Nilsson deformed well were fixed at $\beta=0.30$, $\mu=0.42$, and $\kappa=0.0637$. The orbital emptiness parameters (or pairing factors) V^2 were constrained to satisfy the relation

$$V_i^2=\frac{1}{2}\left(1-\frac{\epsilon_i-\lambda}{[(\epsilon_i-\lambda)^2+\Delta^2]^{1/2}}\right),$$

where $\epsilon_i-\lambda$ is the difference between the single-particle energy ϵ_i of the ith Nilsson orbital and the Fermi energy λ, and Δ is the pairing gap. These latter quantities were determined by identifying bandhead energies, after subtraction of rotational energy, with quasiparticle energies $([(\epsilon_i-\lambda)^2+\Delta^2]^{1/2}-\Delta)$. The bandhead energies, moment of inertia parameters, and, for $K=\frac{1}{2}$ bands, the decoupling parameters were varied in the fitting procedure. As has been noted previously,[26] best results were obtained by reducing Coriolis-coupling matrix elements to 60% of the value calculated by the Nilsson model. Table V lists the final values of bandhead energies, moment of inertia parameters, and decoupling parameters

TABLE I. Optical model parameters used in the distorted-wave calculations. Bound state well parameters are also listed.

	V (MeV)	r_0 (fm)	r_c (fm)	a (fm)	W (MeV)	W_D	r_I (fm)	a_I (fm)	λ_{SO}
d [a]	98.4	1.16	0.74	0.752	10.4	...	1.48	0.957	...
d [b]	102.2	1.15	1.15	0.81		17.6	1.34	0.68	...
t [c]	166.7	1.16	1.40	0.752	14.7		1.498	0.817	...
Bound states	d	1.17	1.17	0.75					25.0

[a] Parameters obtained by fitting deuteron scattering on four deformed targets (discussed in text).
[b] Reference 21.
[c] Reference 20.
[d] Well depth adjusted to give correct separation energy.

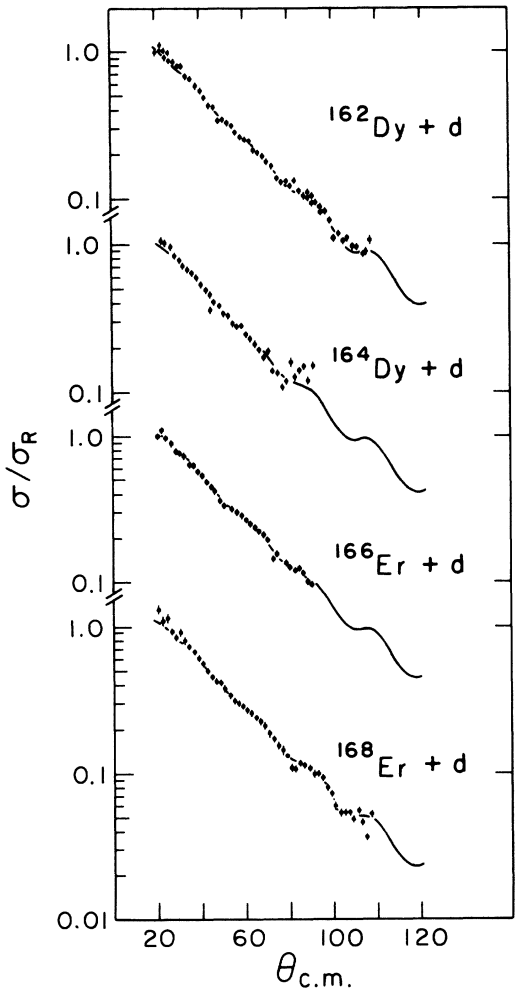

FIG. 16. Angular distributions for elastic scattering of 17 MeV deuterons from several even-even rare-earth nuclides. The solid curves are optical model calculations discussed in the text.

along with the orbital emptiness parameters for all the Nilsson levels considered.

The BANDMIX code further used the Nilsson model parameters determined by the above procedure to calculate spectroscopic factors

$$(C^2S)_J = 2\left(\sum_K a_{jK} C^K_{j,l}\, V_K\right)^2 ,$$

where $C^K_{j,l}$ is the expansion coefficient of the one-quasiparticle Nilsson state in a spherical basis, j is the spin of the state, and the a_{jK} are determined by Coriolis mixing of neighboring single-quasihole states. If Coriolis coupling is neglected the spectroscopic factor reduces to

$$(C^2S)_j = 2(C^K_{j,l})^2 V_K{}^2 .$$

Coriolis coupling is crucial to understanding the intensity patterns of several strongly coupled bands. To show which bands are strongly coupled, spectroscopic factors calculated without Coriolis coupling are included (in parentheses) in Tables III and IV along with the spectroscopic factors for the full calculation.

TABLE II. Quantum numbers of bound state orbitals used to calculate form factors for DWBA calculations.

l	j	n
0	$\frac{1}{2}$	3
1	$\frac{3}{2}$	3
2	$\frac{3}{2}$	2
3	$\frac{5}{2}$	2
4	$\frac{7}{2}$	1
5	$\frac{9}{2}$	1
6	$\frac{13}{2}$	1

TABLE III. Excitation energies for ^{159}Gd levels populated through the ^{160}Gd$(d,t)^{159}$Gd reaction. Nilsson model assignments have been taken from Ref. 8, except where otherwise indicated. l values are those indicated by the angular distribution shape, and for levels whose Nilsson model assignment is not determined, spectroscopic factors correspond to the observed l transfer. Several levels whose Nilsson assignment has been reported in previous work show angular distributions characteristic of l values incompatible with that Nilsson assignment — in these cases spectroscopic factors are shown for both possible l transfers (see text for discussion).

E_X (MeV)	l	Assignment	S_{exp}	S model Mixed	S model (Unmixed)	$d\sigma$ ($\theta = 30°$) $d\Omega$
0.000	1	$\frac{3}{2}\frac{3}{2}^-[521]$	0.144	0.080	(0.072)	0.38
0.049	a	$\frac{5}{2}\frac{3}{2}^-[521]$	0.023	0.014	(0.005)	0.040
0.067	a	$\frac{5}{2}\frac{5}{2}^+[642]$	0.0093	0.0035	(0.0035)	0.05
0.121	3	$\frac{7}{2}\frac{3}{2}^-[521]$	0.45	0.48	(0.50)	0.28
0.146	3	$\frac{5}{2}\frac{5}{2}^-[523]$	0.066	0.028	(0.027)	0.039
0.185	4	$\frac{9}{2}\frac{5}{2}^+[642]$	0.32	0.15	(0.15)	0.18
0.212	5	$\frac{9}{2}\frac{3}{2}^-[521]$	0.32	0.68	(0.35)	0.040
0.226	3	$\frac{7}{2}\frac{5}{2}^-[523]$	0.25	0.20	(0.058)	0.14
0.272	a	$\frac{11}{2}\frac{5}{2}^+[642]$	0.20	0.011	(0.011)	0.0078
0.326	(5)	$\frac{11}{2}\frac{3}{2}^-[521]$	0.33	0.05	(0.068)	0.028
		$\frac{9}{2}\frac{5}{2}^-[523]$		0.15	(0.29)	
0.373	6	$\frac{13}{2}\frac{5}{2}^+[642]$	2.1	1.29	(1.29)	0.066
0.455	b	$\frac{11}{2}\frac{5}{2}^-[523]$	0.26	0.073	(0.020)	0.027
0.507	1	$\frac{1}{2}\frac{1}{2}^-[521]$	0.064	0.057	(0.057)	0.20
0.557	(1)	$\frac{3}{2}\frac{1}{2}^-[521]$	0.0053	0.010	(0.014)	0.017
0.588	3	$\frac{5}{2}\frac{1}{2}^-[521]$	0.070	0.027	(0.041)	0.025
0.602	a					0.015
0.642	a					0.014
0.683	(5) [b]	$\frac{11}{2}\frac{11}{2}^-[505]$	1.35	1.89	(1.89)	0.10
0.704	3	$\frac{7}{2}\frac{1}{2}^-[521]$	0.052	0.074	(0.048)	0.047
0.743	2	$\frac{3}{2}\frac{3}{2}^+[402]$	0.76	1.68	(1.62)	0.70
0.780	0	$\frac{1}{2}\frac{1}{2}^+[660]$	0.15	0.004	(0.004)	0.30
0.799	a					0.027
0.820	a					0.012
0.856	(2) [b]	$\frac{9}{2}\frac{1}{2}^+[660]$ $(0.023; l=2)$	0.042	0.37	(0.37)	0.021
0.876	3	$\frac{5}{2}\frac{5}{2}^-[512]$ [c]	0.035	0.0009	(0.0003)	0.030
0.925	a					0.034
0.946	3	$\frac{7}{2}\frac{5}{2}^-[512]$	0.022	0.046	(0.082)	0.022
0.973	0	$\frac{1}{2}\frac{1}{2}^+[400]$	0.374	1.14	(1.14)	0.64
0.999	2	$\frac{3}{2}\frac{1}{2}^+[660]$	0.19	0.007	(0.0013)	0.16
1.057	(2) [b]	$\frac{13}{2}\frac{1}{2}^+[660]$ $(0.09; l=2)$	1.28	1.45	(1.45)	0.062
1.078	1		0.01			0.020
1.109	1	$\frac{3}{2}\frac{3}{2}^-[532]$	0.05	0.013	(0.097)	0.16
1.128	d					0.087
1.143	1	$\frac{3}{2}\frac{1}{2}^-[530]$	0.19	0.34	(0.26)	0.47

TABLE III *(Continued)*

E_X (MeV)	l	Assignment	S_{exp}	S model Mixed	S model (Unmixed)	$d\sigma$ ($\theta = 30°$) $d\Omega$
1.158	(3)	$\frac{5}{2}\ \frac{3}{2}^-$[532]	0.27	0.54	(0.35)	0.13
1.177	(3)	$\frac{5}{2}\ \frac{1}{2}^-$[530]	0.04	0.001	(0.189)	0.033
1.201	(3) [d]		0.07			0.060
		$\frac{7}{2}\ \frac{1}{2}^-$[530]		0.72	(0.49)	
1.238		$\frac{7}{2}\ \frac{3}{2}^-$[532]	0.10	0.002	(0.35)	0.040
1.251	a					0.015
1.282	b	$\frac{7}{2}\ \frac{1}{2}^+$[660]	0.178	0.0017	(0.0015)	0.067
1.301	b	$\frac{9}{2}\ \frac{1}{2}^-$[530]	0.42	1.4	(0.82)	0.020
1.341	(3) [b]	$\frac{9}{2}\ \frac{3}{2}^-$[532] (0.11; $l = 3$)	0.89	0.13	(0.94)	0.073
1.365	a					0.014
1.391	b	$\frac{11}{2}\ \frac{1}{2}^-$[530]	0.16	0.010	(0.16)	0.022
1.415	a					0.035
1.426	2		0.081			0.063
1.506	e					0.033
1.522	e					0.008
1.540	e					0.030
1.559	a					0.026
1.570	d					0.058
1.578	e					0.022
1.600	e					0.026
1.655	e					0.032
1.668	e					0.032
1.689	e					0.020
1.811	a					0.028
1.839	(2) [d]		0.12			0.052
1.867	a					0.025
1.882	a					0.020
1.961	(3) [b]	$\frac{7}{2}\ \frac{7}{2}^+$[404] (0.4; $l = 3$)	1.19	1.94	(1.94)	0.23
1.978	e					0.015
1.993	d					0.047
2.007	e					0.017
2.030	e					0.080
2.045	e					0.019
2.071	e					0.029
2.089	e					0.053
2.238	e					0.050
2.560	e					0.033

[a] The angular distribution is poorly fitted by any l value, but the level is very weakly populated. Where a Nilsson model assignment is available, spectroscopic factors have been extracted for the model-predicted l value.

[b] Anomalous angular distribution (see Fig. 7).

[c] Assignment from P. Kemnitz *et al.* (Ref. 13).

[d] Strong, unidentified state (see Fig. 8).

[e] Clearly observed in five or more spectra, but populated weakly and/or obscured by impurities or stronger transitions in enough spectra that no meaningful angular distribution was extracted.

V. DISCUSSION

A. Information from spectroscopic factors

Figure 17 compares the measured spectroscopic factors with those predicted by the Nilsson model for members of several rotational bands. Figure 17 includes spectroscopic factors extracted from (d,t) measurements on five rare-earth targets. Except for preliminary reports[27] and a small part of the data which was included in Ref. 7, the data

TABLE IV. Excitation energies for ^{161}Dy levels populated through the ^{162}Dy$(d,t)^{161}$Dy reaction. Nilsson model assignments have been taken from Ref. 9, except where otherwise indicated. l values have been derived from angular distribution shapes and, for levels whose Nilsson model assignment is not determined, spectroscopic factors correspond to the observed l transfer. Several levels whose Nilsson assignment has been reported in previous work show angular distributions characteristic of l values incompatible with that Nilsson assignment—in these cases spectroscopic factors are shown for both possible l transfers (see text for discussion).

E_X	l	Assignment	S_{exp}	S model Mixed	S model (Unmixed)	$d\sigma(\theta=30°)/d\Omega$ (mb/sr)
0.000	a	$\frac{5}{2}\frac{5}{2}^+[642]$		0.0043	(0.0024)	
0.025	3	$\frac{5}{2}\frac{5}{2}^-[523]$	0.076	0.050	(0.044)	0.16
0.045	b	$\frac{7}{2}\frac{5}{2}^+[642]$	0.045	0.0024	(0.0017)	0.15
0.075	1	$\frac{3}{2}\frac{3}{2}^-[521]$	0.12	0.12	(0.10)	0.33
0.100	4	$\frac{9}{2}\frac{5}{2}^+[642]$ [c]	0.16	0.21	(0.10)	0.13
		$\frac{7}{2}\frac{5}{2}^-[523]$		0.008	(0.093)	
0.130	(2) [b]	$\frac{5}{2}\frac{3}{2}^-[521]$ $(0.02;l=2)$	0.06	0.0072	(0.0071)	0.007
0.201	a	$\frac{9}{2}\frac{5}{2}^-[523]$		0.79	(0.47)	
0.213	3	$\frac{7}{2}\frac{3}{2}^-[521]$	0.76	0.99	(0.71)	0.32
0.268	6	$\frac{13}{2}\frac{5}{2}^+[642]$ [c]	1.4	2.0	(0.88)	0.037
0.317	a	$\frac{9}{2}\frac{3}{2}^-[521]$	~0.6	0.39	(0.48)	0.024
0.369	1	$\frac{1}{2}\frac{1}{2}^-[521]$	0.08	0.072	(0.072)	0.19
0.418	1	$\frac{3}{2}\frac{1}{2}^-[521]$	0.02	0.014	(0.018)	0.029
0.445	(3)	$\frac{5}{2}\frac{1}{2}^-[521]$	0.07	0.043	(0.053)	0.086
0.487	5 [b]	$\frac{11}{2}\frac{11}{2}^-[505]$	1.52	1.84	(1.84)	0.059
0.510	d					0.024
0.521	e					0.030
0.552	2	$\frac{3}{2}\frac{3}{2}^+[402]$ [f]	0.78	1.62	(1.56)	0.53
0.569	(3)	$\frac{7}{2}\frac{1}{2}^-[521]$	0.09	0.076	(0.060)	0.050
0.609	0	$\frac{1}{2}\frac{1}{2}^+[400]$ [f]	0.39	1.11 [f]	(1.11)	0.40
0.632	(2) [b]	$\frac{9}{2}\frac{1}{2}^-[521]$ $(0.06;l=2)$	0.66	0.11	(0.068)	0.025
0.680	2	$\frac{3}{2}\frac{3}{2}^+[651]$ [f]	0.16	0.0011	(0.0006)	0.091
0.718	4		0.05			0.040
0.733	e					0.044
0.775	0	$\frac{1}{2}\frac{1}{2}^+[400]$ [f]	0.37	1.11 [f]	(1.11)	0.37
0.805	(1) [b]	$\frac{11}{2}\frac{1}{2}^-[521]$ $(0.01;l=1)$	0.50	0.015	(0.0078)	0.020
0.828	2		0.05			0.31
0.850	2		0.18			0.18
0.860	1	$\frac{3}{2}\frac{1}{2}^-[530]$	0.18	0.24	(0.25)	0.31
0.880	a	$\frac{5}{2}\frac{1}{2}^-[530]$	~0.1	0.18	(0.18)	0.046
0.925	3		0.04			0.020
0.960	b	$\frac{7}{2}\frac{1}{2}^-[530]$	0.16	0.35	(0.47)	0.029
0.971	d					0.022
0.980	d					0.006
1.005	d					0.010

TABLE IV *(Continued)*

E_X	l	Assignment	S_{exp}	S model Mixed	S model (Unmixed)	$\frac{d\sigma(\theta=30°)}{d\Omega}$ (mb/sr)
1.028	2		0.06			0.044
1.127	a					0.006
1.135	3		0.05			0.031
1.143	3		0.05			
1.158	1		0.01			0.024
1.182	0		0.01			0.014
1.209	3		0.05			0.032
1.274	3		0.05			0.022
1.290	d					0.020
1.362	a					0.021
1.380	1		0.03			0.068
1.417	(2)	$\frac{7}{2}\ \frac{7}{2}^+[404]$	1.4	0.92	(0.92)	
1.436	1		0.03			0.063
1.459	d					0.013
1.601	0		0.04			0.026
1.650	d					0.013
1.743	0		0.01			0.017
1.765	a					0.018
1.780	0		0.01			0.025
1.818	0		0.02			0.040
1.859	d					0.022
1.871	d					0.036
1.892	3		0.08			0.034
1.920	e					0.034
2.215	3		0.06			0.031
2.230	d					0.020

[a] Clearly observed in five or more spectra, but populated weakly and/or obscured by impurities or stronger transitions in enough spectra that no meaningful angular distribution was extract.

[b] Anomalous angular distribution (see Fig. 14).

[c] Assignment from Ref. 15.

[d] The angular distribution is poorly fitted by any l value but the level is very weakly populated. Where a Nilsson model assignment is available, spectroscopic factors have been extracted for the model-predicted l value.

[e] Strong, unidentified state (see Fig. 15).

[f] Almost certainly has strong $\Delta N=2$ mixing; model spectroscopic factor is an upper limit.

from three of these systems are, as yet, unpublished. However, it seems worthwhile to include all these systems in Fig. 17 to provide a perspective for the spectroscopy and reaction mechanism discussion below. The Nilsson bands in Fig. 17 are arranged in order of increasing energy and it is possible to follow the shift of the Fermi energy to the right of the figure as neutron number increases from 95 (^{159}Gd and ^{161}Dy) to 99 (^{167}Er). Spectroscopic factors marked with an A in Fig. 17 correspond to transitions which exhibited anomalous angular distributions. These result from fitting the DWBA cross sections to the average level of the poorly fit experimental angular distributions and are inherently more uncertain than the other spectroscopic factors shown in the figure. Results for members of four positive parity bands ($\frac{1}{2}^+[400]$, $\frac{1}{2}^+[660]$, $\frac{3}{2}^+[402]$, and $\frac{3}{2}^+[651]$) are not included in Fig. 17 because these bands are well known[28] to show signs of strong $\Delta N=2$ mixing (see discussion below) and are not well fitted in any of the five residual nuclides. Spectroscopic factors for members of these bands are, however, included in Tables III and IV. While Fig. 17 and Tables III and IV show that many transitions are observed to agree with the Nilsson model predictions, there are obviously many disagreements as well. Even assuming a one-step direct reaction mechanism several factors make interpreting these discrepancies difficult: (1) The structure of positive parity levels in these residual nuclei is complicated by $\Delta N=2$ mixing, i.e., two downward sloping (with increasing deformation) $N=6$ orbitals, $\frac{1}{2}^+[660]$ and $\frac{3}{2}^+[651]$, encounter two upward sloping $N=4$ orbit-

TABLE V. Bandhead energies, moment of inertia parameters, decoupling parameters, and level fullness parameters, V^2, from fitting the energy spectra of ^{159}Gd and ^{161}Dy as described in the text.

Nuclide	Nilsson band	Bandhead energy (keV)	Moment of inertia parameter (keV)	Decoupling parameter	V^2
^{159}Gd	$\frac{3}{2}^-[521]$	0	11.4		0.50
	$\frac{5}{2}^-[523]$	146	11.2		0.20
	$\frac{1}{2}^-[521]$	507	11.7	0.45	0.11
	$\frac{11}{2}^-[505]$	683	a		0.95
	$\frac{5}{2}^-[512]$	876	10.5		0.055
	$\frac{1}{2}^-[530]$	b	7.7	0.17	0.96
	$\frac{3}{2}^-[532]$	b	9.8		0.96
	$\frac{5}{2}^+[642]$	67	7.6		0.73
	$\frac{3}{2}^+[402]$	743	a		0.93
	$(+\frac{3}{2}^+[651])$				
	$\frac{1}{2}^+[400]$	973	a	c	0.95
	$\frac{1}{2}^+[660]$	780	13.3	4.56 [c]	0.94
	$(+\frac{1}{2}[400])$				
^{161}Dy	$\frac{5}{2}^-[523]$	25	11.2		0.32
	$\frac{3}{2}^-[521]$	75	12.5		0.70
	$\frac{1}{2}^-[521]$	369	11.8		0.14
	$\frac{11}{2}^-[505]$	487	a		0.92
	$\frac{1}{2}^-[530]$	b	6.6		0.93
	$\frac{5}{2}^-[512]$	b	14.6		0.080
	$\frac{5}{2}^+[642]$	0	7.8		0.50
	$\frac{3}{2}^+[402]$ $\frac{3}{2}^+[651]$	552	c		0.90
	$\frac{1}{2}^+[400]$ $\frac{1}{2}^+[660]$	609	c	c	0.93

[a] Not well determined because too few members of the band were observed.
[b] Bandhead not observed.
[c] Strong $\Delta N = 2$ mixing makes these parameters very uncertain.

als, $\frac{1}{2}^+[400]$ and $\frac{3}{2}^+[402]$ just below the $N=95$ Fermi surface.[28] The interactions between pairs of levels based on orbitals such as these have been studied[29] but are not at all well established. (2) The Nilsson model spectroscopic strengths are in many cases strongly dependent on the assumed strength of the Coriolis-coupling matrix elements. As is mentioned above, the observed energy spectrum is not well reproduced unless these matrix elements are reduced to ~ 60% of their pure Nilsson model values. This prescription has evolved from results of many experiments[26] and has received further support from the attempts of Damgaard, Kusuno, and Faessler[30] to explain backbending of yrast bands. This 60% reduction of the Coriolis coupling seems currently the most reasonable procedure, and there are equally great or greater discrepancies between the experimental spectroscopic factors and those resulting from Nilsson model calculations either without Coriolis coupling (shown in parentheses in Tables III and IV) or with full Coriolis coupling. However, this sensitivity of the model spectroscopic factors to the assumed strength of the Coriolis coupling adds

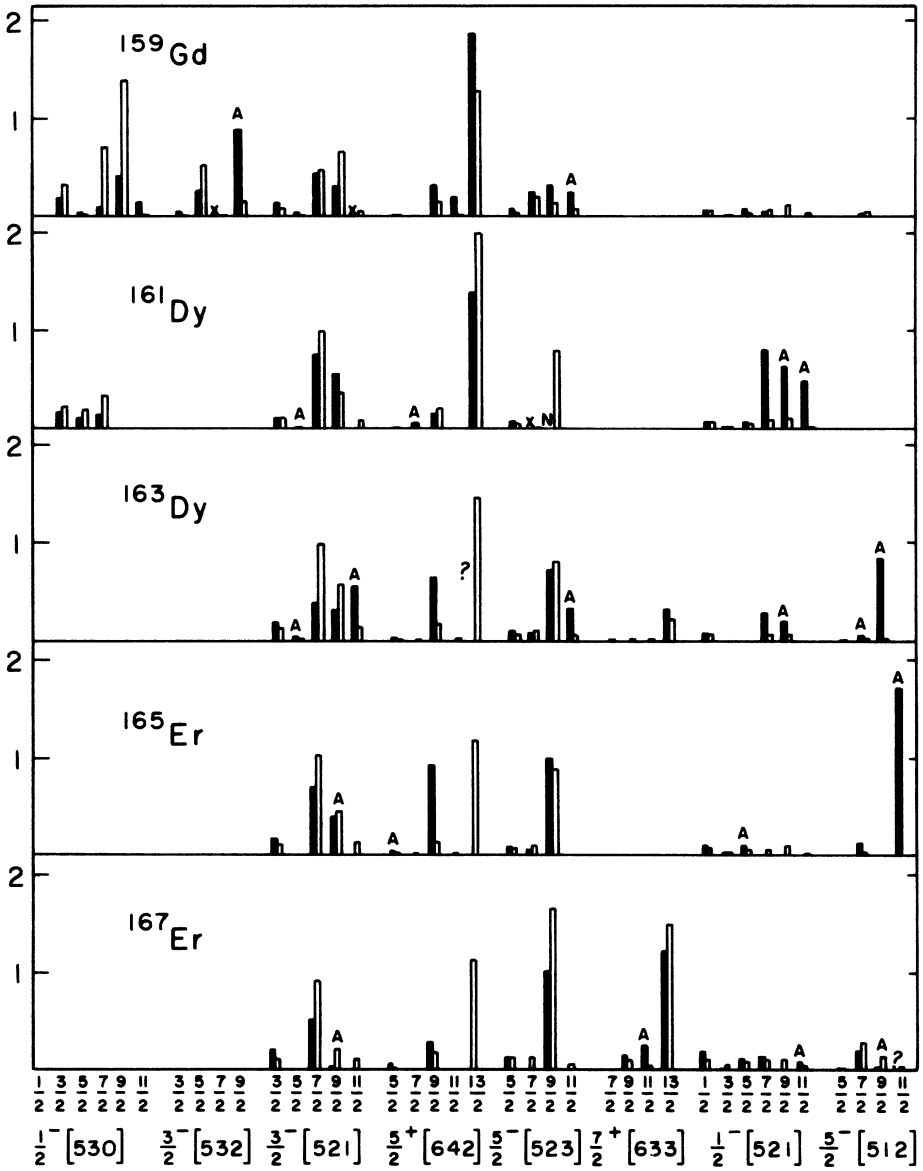

FIG. 17. The solid bars represent experimental spectroscopic factors for (d,t) population of the indicated states. The open bars represent spectroscopic factors predicted by the Nilsson model calculation described in the text. The excitation energy of the Nilsson model single-particle states increases from left to right along the abscissa so the Fermi level shifts to the right as neutron number increases from 95 at the top of the figure to 99 at the bottom. The four positive parity bands which are subject to strong $\Delta N = 2$ mixing are not included in the figure (see text for discussion).

another source of uncertainty to interpreting the spectroscopic factor discrepancies seen in Tables III and IV and Fig. 17. (3) As is discussed above, the form factors used in the DWBA analysis were calculated with spherical Woods-Saxon binding wells whose depth was adjusted according to the binding energy prescription (with no configuration mixing). Such a procedure is only justifiable for a single particle outside a closed shell; normalizing such a wave function almost certainly introduces distortions in the form factor at the surface of the deformed nuclides considered here. Rost has calculated couplings between channels in the expansion of a deformed single-particle wave function and has found sizeable changes in normalization of individual form factors at the nuclear surface.[31] Unfortunately, the application of Rost's procedure is not only difficult, but also involves

an interplay between the assumed details of the structure of each nuclear state and the reaction mechanism assumptions. As was stated above, the conventional DWBA is used to organize the experimental results of this investigation and further, model-dependent adjustments of the form factors used in the analysis would be inappropriate.

The above-mentioned difficulties with $\Delta N = 2$ mixing, Coriolis coupling, and form factor normalizations certainly restrict the conclusions which can be drawn from comparing the experimental spectroscopic factors with those predicted by the Nilsson model calculation. However, the Coriolis-coupling prescription employed herein is probably reasonable and Rost's estimate[31] indicates that the form factor normalization problems only introduce ~30% extra uncertainty in the more troublesome cases. So most of the spectroscopic factors for the negative parity levels shown in Fig. 17 and Tables III and IV should probably agree within $\lesssim 50\%$ with the Nilsson model expectations. Many of these spectroscopic factors disagree with the model by a factor of 2 or more, and either this indicates unexpectedly strong vibration-quasiparticle mixing,[32] or it indicates that many of these transitions do not proceed as pure one-step direct transfers.

Spectroscopic factor sums for each l value are listed in Table VI. These have been compiled on the assumption that all Nilsson model assignments listed in Tables III and IV—including those levels discussed below as showing anomalous or incompatible l angular distributions—have been correctly identified. These spectroscopic factor sums agree well with the model calculations. (Even though the ^{161}Dy spectrum is more compressed than that of ^{159}Gd, more Nilsson bands are identifiable in ^{159}Gd and so the model calculation for ^{159}Gd allows a larger summed limit, ~15. Additional pickup strength for ^{161}Dy may well be spread over many vibrationally coupled states—indeed, both Tables III and IV show many weak nondescript angular distributions, denoted by footnotes a and d, respectively, which could be associated with transitions to vibrational levels.[32] In any case the less compressed ^{159}Gd spectrum shows more angular distributions which appear to fit into the Nilsson scheme.)

For the even l value strengths the good agreement between observation and the model is almost certainly fortuitous—especially for the $l = 0$ strength in ^{161}Dy which is fragmented over seven states rather than the two expected from the Nilsson model and observed in ^{159}Gd. This fragmentation of $l = 0$ strength probably arises from a vibrational coupling. Most of $l = 4$ strength for each nucleus resides in the expected $\frac{7}{2}^+[404]$ hole state.

TABLE VI. Summed spectroscopic strengths for all observed l values. States identified in Tables III and IV with a rotational band built on a specified Nilsson level are assumed to be correctly identified. Strengths of transitions to previously unidentified states whose angular distributions show characteristic l patterns have also been included. The model predictions include the Nilsson states listed in Table V and since more Nilsson states are included for ^{159}Gd than for ^{161}Dy, the model sum limits are different.

	^{159}Gd		^{161}Dy	
l	Expt.	Model	Expt.	Model
0	0.52	1.1	0.85	1.1
1	0.45	0.49	0.60	0.32
2	1.1	1.7	1.1	1.6
3	1.4	2.2	1.7	2.6
4	1.7	2.5	1.6	1.1
5	3.7	4.4	3.3	2.3
6	3.6	2.8	1.4	2.0
Sum	12.5	15.2	10.6	11.0

Both previously identified $\frac{7}{2}^+[404]$ bandheads lie at high excitation energy where strong vibrational coupling might occur and both these transitions are among those discussed below as showing angular distributions which can be fitted with an l value incompatible with their model assignment.

Over-all the spectroscopic factor sums are in surprisingly good agreement with Nilsson model expectations. This was also the case for the 12 MeV (d,t) work where this agreement combined with the lack of complete angular distributions,[8,9] seemed to indicate that the DWBA assumptions and the Nilsson model meshed well to account for the data. Several of the available 12 MeV angular distributions did show deviations from DWBA predicted shapes[10]; an attempt was made to make an approximate correction to the DWBA for multistep effects[33]; and the Nilsson band "signatures" in the individual spectra of Refs. 8 and 9 did show several large discrepancies of the sort shown in Fig. 17. But the surprising over-all spectroscopic factor agreement (which arises partly from approximate equality of DWBA-predicted peak cross sections and average cross sections for transitions whose angular distributions frequently bear little or no resemblance to DWBA expectations) has tended to foster a confidence in the simplest DWBA + Nilsson model analysis that many of the considerations discussed above would not support.

Interesting and more reliable results, in regard both to the spectroscopy of ^{159}Gd and ^{161}Dy and to the mechanism for population of these nuclides through the (d,t) reaction, can be extracted from the shapes of the observed angular distributions

with only occasional appeal to spectroscopic factors for ancillary evidence.

B. Spectroscopic information from angular distribution shapes

The anomalous angular distributions (those whose shape is not well fitted by DWBA calculations which use an l value which is consistent with the previously assigned angular momentum parity of the state) are grouped in Figs. 7, 13, and 14. While most of these angular distributions cannot be fitted with DWBA calculations for any l value, several can be fitted under the assumption that the previous work misidentified the state. In ^{159}Gd these states are: 1.057 MeV (previously assigned $\frac{13}{2}$ member of the $\frac{1}{2}^+[660]$ band; currently fit with $l=2$); 1.341 MeV (previously assigned $\frac{9}{2}$ member of the $\frac{3}{2}^-[532]$ band; currently fit with $l=3$); and 1.961 MeV (previously assigned $\frac{7}{2}$ member of $\frac{7}{2}^+[404]$ band; currently fit with $l=3$). Additionally, the transition to the previously assigned $\frac{9}{2}$ member of the $\frac{1}{2}^+[660]$ band at 0.856 MeV bears some resemblance to DWBA $l=2$ angular distribution and has no resemblance to an $l=4$ angular pattern. These four angular distributions are shown in Fig. 7 with solid lines for the DWBA curves appropriate to the previous assignment and dashed curves for the best fit l calculation.

In ^{161}Dy there are also four anomalous angular distributions which can be explained as l value misassignments: the 0.130 MeV state (previously called the $\frac{5}{2}$ member of the $\frac{3}{2}^-[521]$ band; presently better fit with $l=2$); the 0.632 MeV state (previously called the $\frac{9}{2}$ member of the $\frac{1}{2}^-[521]$ band; presently better fit with $l=2$); the 0.805 MeV state (previously called the $\frac{11}{2}$ member of the $\frac{1}{2}^-[521]$ band; presently better fit with $l=1$); and the 1.420 MeV state (previously called the $\frac{7}{2}$ member of the $\frac{7}{2}^+[404]$ band; presently better fit with $l=2$). The angular distributions for these four transitions appear in Fig. 14 with best l calculations shown as dotted curves and previously assigned l calculations as solid curves.

Obviously any of the above examples of possible l assignment changes could result from a truly anomalous angular distribution—one that the DWBA calculation shouldn't be able to fit. But most of them are probably misassignments arising from the use of model-dependent interpretations of individual spectra from charged particle experiments or, in the case of levels whose spins have been assigned from γ decay experiments, misassignments arising from (d,t) population of a different spin level which lies close in excitation energy to the previously observed level. Members of the $\frac{1}{2}^-[521]$ and $\frac{3}{2}^-[521]$ levels are particularly likely to fall into the first category since some member of each of these bands[7] exhibits a genuinely anomalous (fit by no DWBA curve) angular distribution in each of the five nuclides populated in this series of experiments. The levels in ^{161}Dy are more likely to be multiplets than those in ^{159}Gd because of the well-known compression of the spectrum of Nilsson single-quasineutron orbitals as Z increases.[9] This spectral compression with Z also affects the model-predicted spectroscopic factors through increased Coriolis-coupling effects which affect the pattern of spectroscopic factors for population of members within a given rotational band. This increased band mixing should be quite reasonable, but to date theoretical attempts to understand the Z-dependent spectral compression have been unsuccessful.[34]

C. Implications of angular distribution shapes for understanding the reaction mechanism

As was reported in Ref. 7 there are several Nilsson bands of which at least one member exhibits an anomalous angular distribution in at least four of the five residual nuclides ^{159}Gd, ^{161,163}Dy, and ^{165,167}Er. These bands are: $\frac{11}{2}^-[505]$, $\frac{5}{2}^+[642]$, $\frac{1}{2}^-[521]$, and $\frac{3}{2}^-[521]$. The $\frac{1}{2}^-[521]$ and $\frac{3}{2}^-[521]$ bands also tend to exhibit somewhat greater discrepancies between experimental and model spectroscopic factors than do members of other bands, but this effect is difficult to assess in view of the spectroscopic factor uncertainties discussed above. In ^{160}Gd the $\frac{1}{2}^-[521]$ band lies far above the Fermi surface (see Fig. 17) and thus is not strongly populated as a hole state in ^{160}Gd$(d,t)^{159}$Gd. Both $l=1$ angular distributions to members of this band (Fig. 3) in ^{159}Gd show evidence of oscillations not predicted by the DWBA calculations. Angular distribution effects of this kind have been used (in conjunction with CCBA calculations) as evidence for a breakdown of the one-step direct mechanism,[1] but since it has not been possible to perform CCBA calculations in the present work these angular distributions were not regarded as anomalous in Ref. 7 and have not been listed as anomalous in Table III or Fig. 17. The $\frac{3}{2}^-[521]$ band is near the Fermi surface for ^{160}Gd and its members are appreciably populated in ^{159}Gd. Only one of these transitions (the $\frac{11}{2}^-$ state at 0.326 MeV) shows any evidence of anomalous behavior (Fig. 7) and this evidence is ambiguous since this state should be the weakly populated member of an unresolved $l=5$ doublet. As can be seen from Fig. 17, the $\frac{1}{2}^-[521]$ and $\frac{3}{2}^-[521]$ bands show unambiguous anomalies in each of the other four residual nuclides. In ^{161}Dy (Fig. 14) the anomalous members of these bands can be interpreted as misassigned l states, as was dis-

cussed above, but this is generally not the case[7] for ^{163}Dy and ^{165,167}Er.

As was noted above, many of the easily identified anomalous angular distributions shown in Figs. 7, 13, and 14 are high l cases which have large cross sections at small angle. Attributing this filling in of the expected small-angle minimum to multistep processes seems reasonable because most inelastic transitions that could contribute to the population of these high spin levels by multistep routes would tend to reduce the l which is transferred with the neutron and these l reductions could plausibly fill in the forward angle cross section.

Several of the anomalous angular distributions shown in Figs. 7 and 14 show strong oscillations at small angles. (This is true of the ^{159}Gd states at 1.282, 1.301, and 1.391 MeV and possibly of the ^{159}Gd state at 0.856 MeV. It is true of the ^{161}Dy state at 0.045 MeV and also, if the previous spin assignments were correct, of the states at 0.130 and 0.805 MeV in ^{161}Dy.) Such structure is very similar to that reported by Ascuitto, King, and McVay[1] in CCBA calculations for ^{186}W(d,p) and ^{172}Yb(d,p) transitions. Similar, but generally less pronounced, oscillatory behavior is superimposed at larger angles on several angular distributions whose gross features are otherwise well fitted by DWBA calculations; notable examples of such angular distributions are those populating the states at: 0.946 and 1.177 MeV (Fig. 4) and 0.185 MeV (Fig. 6) in ^{159}Gd and 0.445 and 0.925 MeV (Fig. 12) and 1.158 MeV (Fig. 10) in ^{161}Dy.

It is obviously of interest to try to understand why some transitions exhibit angular distribution patterns that agree well with DWBA predictions while others deviate so markedly as those discussed above. Cotanch and Vincent[35] have recently developed a method to approximate CCBA calculations which not only requires less computer time than does a full CCBA calculation but which also may allow greater insight into the sensitive features of the calculation. Hopefully the results of this investigation will provide a suitable data base for an investigation of the structure and/or dynamical conditions under which the one-step DWBA assumptions break down.

VI. SUMMARY AND CONCLUSIONS

The shapes of angular distribution from the (d,t) population of states in ^{159}Gd and ^{161}Dy are generally well fitted by DWBA calculations, but a significant number of angular distributions either cannot be fitted with any DWBA calculation or can only be fitted with a DWBA calculation which assumes a different l transfer than would be required if the previously determined angular momentum parity of the residual state were correct. Another group of angular distributions is qualitatively fitted by the expected DWBA diffraction patterns but these distributions show rapid oscillations superimposed on the basic l-dependent structure; this effect is reminiscent of structure in ^{172}Yb and ^{186}W(d,p) data which Ascuitto *et al.*[1] fitted with CCBA calculations. Since Cotanch and Vincent[35] have recently developed a method to approximate CCBA calculations (in a format which may allow one to test for the sensitive features of the calculation without using excessively large amounts of computer time), it is hoped that the results of this investigation will provide a suitable data base for an investigation of the structure and/or dynamical conditions under which the one-step DWBA assumptions are applicable.

The spectroscopic factors extracted from the DWBA analysis of the presently reported angular distributions are not in very good agreement with Nilsson model predictions—even for the levels whose angular distributions are rather well fitted. These factor of ~2 discrepancies cannot be entirely ascribed to multistep transfer processes because of uncertainties in the treatment of the deformed form factor in the DWBA analysis of the data and sensitivity of the model-predicted spectroscopic factors to uncertainties in assumed Coriolis-coupling strengths and $\Delta N = 2$ wave function admixtures.

ACKNOWLEDGMENTS

We appreciate the hospitality of Dr. J. R. Erskine in providing the code BANDFIT and allowing us to use the Argonne automatic plate scanner. We also acknowledge Dr. R. M. Drisko and Dr. C. M. Vincent for several helpful discussions.

*Work supported by the National Science Foundation.

[1] R. J. Ascuitto, C. H. King, and L. J. McVay, Phys. Rev. Lett. 29, 1106 (1972).

[2] R. J. Ascuitto and N. K. Glendenning, Phys. Rev. 181, 1396 (1969); N. K. Glendenning and R. S. Mackintosh, Nucl. Phys. A168, 575 (1971).

[3] A. K. Abdallah, T. Udagawa, and T. Tamura, Phys. Rev. C 8, 1855 (1973); D. K. Olsen, T. Udagawa, T. Tamura, and R. E. Brown, *ibid.* 8, 609 (1973).

[4] N. Austern, *Direct Nuclear Reaction Theories* (Wiley-Interscience, New York, 1970), and references therein; S. K. Penny and G. R. Satchler, Nucl. Phys. 53, 145

(1964).
[5]B. Elbek and P. J. Tjom, in *Advances in Nuclear Physics*, edited by M. Baranger and E. Vogt (Plenum, New York, 1969), Vol. III, and references therein.
[6]M. E. Bunker and C. W. Reich, Rev. Mod. Phys. 43, 348 (1971).
[7]J. V. Maher, G. H. Wedberg, J. J. Kolata, J. C. Peng, and J. L. Ricci, Phys. Rev. C 8, 2390 (1973).
[8]P. O. Tjom and B. Elbek, K. Dan. Vidensk. Selsk., Mat.—Fys. Medd. 36, No. 8 (1967).
[9]T. Grotdal, K. Nybo, and B. Elbek, K. Dan. Vidensk. Selsk., Mat.—Fys. Medd. 37, No. 12 (1970); M. J. Bennett, Ph. D. thesis, Florida State Univ., 1967 (unpublished).
[10]M. Jaskola, K. Nybo, P. O. Tjom, and B. Elbek, Nucl. Phys. A96, 52 (1967).
[11]T. Grotdal, K. Nybo, O. Straume, and T. Thorsteinsen, Physica Norvegica 8, 23, 33 (1975).
[12]M. Bonitz and N. J. S. Hansen, Nucl. Phys. A111, 551 (1968).
[13]P. Kemnitz, L. Funke, K.-H. Kaun, H. Sodan, and G. Winter, Nucl. Phys. A137, 679 (1969).
[14]R. T. Brockmeier and J. D. Rogers, Nucl. Phys. 67, 428 (1965); L. Funke, H. Graber, K.-H. Kaun, H. Sodan, and L. Werner, *ibid.* 55, 401 (1964); V. Berg and S. G. Malmskog, *ibid.* A135, 401 (1969).
[15]S. A. Hjorth, A. Johnson, and G. Ehrling, Nucl. Phys. A184, 113 (1972).
[16]J. R. Erskine and R. H. Vonderohe, Nucl. Instrum. Methods 181, 221 (1970).
[17]J. R. Comfort, ANL Physics Division Informal Report No. PHY-1970B, 1970 (unpublished); P. Spink and J. R. Erskine, ANL Physics Division Informal Report No. PHY-1965B (unpublished).
[18]F. G. Perey (unpublished).
[19]P. D. Kunz, Univ. of Colorado (unpublished).
[20]E. R. Flynn, D. D. Armstrong, J. G. Beery, and A. G. Blair, Phys. Rev. 182, 1113 (1969).
[21]C. M. Perey and F. G. Perey, Phys. Rev. 132, 755 (1963).
[22]W. W. Daehnick and R. M. DelVecchio, Phys. Rev. C 11, 623 (1975).
[23]W. T. Pinkston and G. R. Satchler, Nucl. Phys. 72, 641 (1965); R. J. Philpott, W. T. Pinkston, and G. R. Satchler, ibid. A125, 176 (1969), and references contained therein.
[24]S. G. Nilsson, K. Dan. Vidensk. Selsk., Mat.—Fys. Medd. 29, No. 16 (1955).
[25]J. R. Erskine, Argonne National Laboratory (unpublished).
[26]R. F. Casten, P. Kleinheinz, P. J. Doly, and B. Elbek, Phys. Rev. C 3, 1271 (1971); K. Dan. Vidensk. Selsk., Mat.—Fys. Medd. 38, No. 13 (1972), and references therein.
[27]J. L. Ricci, G. H. Wedberg, J. C. Peng, J. J. Kolata, and J. V. Maher, Bill. Am. Phys. Soc. 18, 581 (1973); 17, 558 (1972).
[28]R. K. Sheline, M. J. Bennett, J. W. Dawson, and Y. Shida, Phys. Lett. 26B, 14 (1968); I. Kanesträm, P. O. Tjöm, and J. Bang, Nucl. Phys. A164, 664 (1971).
[29]B. L. Anderson, Nucl. Phys. A196, 547 (1972), and references therein.
[30]J. Damgaard, S. Kusono, and A. Faessler, Nucl. Phys. A243, 492 (1975).
[31]E. Rost, Phys. Rev. 154, 994 (1967).
[32]V. G. Soloviev and P. Vogel, Nucl. Phys. A92, 449 (1967); and references therein.
[33]M. Jaskola and M. Kozlowski, Acta Phys. Polon. B3, 299 (1972).
[34]V. G. Soloviev, P. Vogel, and G. Jungclaussen, Izv. Akad. Nauk SSSR, Ser. Fiz. 31, 518 (1967) [Bull. Acad. Sci. USSR, Phys. Ser. 31, 515 (1967)].
[35]S. R. Cotanch and C. M. Vincent, Phys. Rev. Lett. 36, 21 (1976).